Study on Numerical Dispersion Error of Hybrid CIP-FDTD Method

Chakarothai JERDVISANOP†   Qiang CHEN   Kunio SAWAYA

Department of Electrical and Communication Engineering, School of Engineering,
Tohoku University. E-mail: †jerd@ecei.tohoku.ac.jp .

Abstract Although the contrained interpolation profile (CIP) method has a smaller numerical dispersion when compared with the standard Yee's finite difference time domain (FDTD) algorithm, the electric and magnetic field arrangements of CIP method make it difficult to model antennas into the analysis space. A hybridization of CIP method and FDTD method was developed to solve the problems of large- or long-distance propagation space including antennas. After the boundary conditions between CIP and FDTD method was validated, then the numerical experiment is performed. The results show that the numerical dispersion of the hybrid CIP-FDTD method is almost same as that of the CIP method, which is superior to that of the FDTD method.

Keywords electromagnetic wave propagation, phase error, CIP, FDTD, numerical analysis, hybrid method

1 Introduction

Recently, there has been a tremendous progress in the field of computational electromagnetics. Most of efforts are required to numerically solve the time-dependent Maxwell equations for propagating and scattering electromagnetic waves. Some of the well-known schemes are the Finite Difference Time Domain (FDTD) method[1], the Finite Element Method (FEM)[2], the Method of Moment (MoM)[3], and so forth. The FDTD method has been widely used because it is easy to implement current sources, dielectrics and conductors instinctively into the calculation. In the FDTD method, the spatial derivatives in Maxwell equations are approximated by finite differences. In the conventional Yee algorithm, electric and magnetic field components are located in the leapfrog arrangement. It has a second-order accuracy in both space and time. Therefore, it gives very satisfactory results if the spatial discretization is fine enough. The most suitable solution for discretization is empirically known that 10-20 cells per wavelength at the highest frequency being simulated is required to obtain the accurate results. However, Yee's FDTD method suffers from numerical dispersion: the numerical velocity of propagation is dependent on the mesh size and the time step size. Since the velocity is a function of the direction of travel because of the cubic Yee's cell, the discretized medium is anisotropic. This anisotropy gives rise to a direction-dependent phase error.[4] These errors are accumulated as the numerical wave propagates, limiting the accuracy of FDTD for solving some problems, such as a long-distance propagation problem.

To reduce the error accumulation and increase the accuracy of time-domain solutions, reducing the grid density can be utilized but it costs more memory sizes and a longer CPU running time to calculate the same model because a smaller cell size implies many more cells to fill a volume of the analysis space. Consequently, many researchers have tried to develop new FDTD algorithms that have smaller dispersion errors than Yee's for a given mesh density. The one of this solutions is a larger computational stencil or higher-order finite differences method such as Ty(2,4) or Ty(2,6) scheme.[5, 6, 7] However, the complexity of computation is increased and more complex treatments of the absorbing boundary condition are required.

Therefore, to reduce the anisotropy of analysis space, the application of the characteristic-based Contrained Interpolation Profile (CIP) method to the computational electromagnetics was proposed by Yabe and co-workers.[8, 9, 10] Since the CIP method can accurately solve the hyperbolic equations, the CIP method can be applied to the propagation of characteristics that appears in electromagnetic waves. Moreover, the CIP scheme is a small-dispersion and stable scheme with third-order accuracy in space[11]. This scheme has been successfully applied to various complex fluid flow problems.[12] And many researchers have tried to apply CIP scheme to solve the electromagnetic problems.[13, 14, 15, 16] Although there are many examples of the applications of the CIP scheme to compute the long-distance propagation of electromagnetic waves, the arrangement of electric and magnetic fields which exist at the same location in the CIP scheme makes it difficult to define a current source, so that it is difficult to model antennas in the region of the CIP scheme.

In this paper, a stable hybridization of the CIP and FDTD methods was performed by applying the newly proposed boundary condition between two regions in the two-dimensional space. In the total analysis region, the antennas are modelled in the FDTD region and empty space for wave propagation is implemented by the CIP scheme. The quantity of reflectivity of the boundary is numerically computed to verify the hybrid method. Moreover the numerical dispersions, defined

as the phase error, of the hybrid CIP-FDTD method is consequently compared to that of the FDTD and CIP method and discussed in this paper.

2 CIP scheme for Maxwell equations

The characteristic-based formulation of the Maxwell equations was derived by Shang[17] as followings. First, the time-dependent Maxwell equations for electromagnetic fields in free space can be generally written in the following form:

$$\nabla \times \mathbf{E} = -\mathbf{J}^* - \frac{\partial \mathbf{B}}{\partial t}, \tag{1}$$

$$\nabla \times \mathbf{H} = \mathbf{J} + \frac{\partial \mathbf{D}}{\partial t}. \tag{2}$$

These equations can be written in flux vector form in a Cartesian frame as

$$\frac{\partial \mathbf{U}}{\partial t} + \mathbf{A}\frac{\partial \mathbf{U}}{\partial x} + \mathbf{B}\frac{\partial \mathbf{U}}{\partial y} + \mathbf{C}\frac{\partial \mathbf{U}}{\partial z} + \mathbf{D}\mathbf{U} = 0, \tag{3}$$

where the coefficient matrices $\mathbf{A}, \mathbf{B}, \mathbf{C}$ and $\mathbf{D}$ are

$$\mathbf{A} = \begin{bmatrix} 0 & 0 & 0 & 0 & 0 & 0 \\ 0 & 0 & 0 & 0 & 0 & 1/\epsilon \\ 0 & 0 & 0 & 0 & -1/\epsilon & 0 \\ 0 & 0 & 0 & 0 & 0 & 0 \\ 0 & 0 & -1/\mu & 0 & 0 & 0 \\ 0 & 1/\mu & 0 & 0 & 0 & 0 \end{bmatrix}, \tag{4}$$

$$\mathbf{B} = \begin{bmatrix} 0 & 0 & 0 & 0 & 0 & -1/\epsilon \\ 0 & 0 & 0 & 0 & 0 & 0 \\ 0 & 0 & 0 & 1/\epsilon & 0 & 0 \\ 0 & 0 & 1/\mu & 0 & 0 & 0 \\ 0 & 0 & 0 & 0 & 0 & 0 \\ -1/\mu & 0 & 0 & 0 & 0 & 0 \end{bmatrix}, \tag{5}$$

$$\mathbf{C} = \begin{bmatrix} 0 & 0 & 0 & 0 & 1/\epsilon & 0 \\ 0 & 0 & 0 & -1/\epsilon & 0 & 0 \\ 0 & 0 & 0 & 0 & 0 & 0 \\ 0 & -1/\mu & 0 & 0 & 0 & 0 \\ 1/\mu & 0 & 0 & 0 & 0 & 0 \\ 0 & 0 & 0 & 0 & 0 & 0 \end{bmatrix}, \tag{6}$$

$$\mathrm{Diag}(\mathbf{D}) = \left\{ \frac{\rho}{\epsilon}, \frac{\rho}{\epsilon}, \frac{\rho}{\epsilon}, \frac{\rho^*}{\mu}, \frac{\rho^*}{\mu}, \frac{\rho^*}{\mu} \right\}, \tag{7}$$

$$\mathbf{U} = [E_x \ E_y \ E_z \ H_x \ H_y \ H_z]^T, \tag{8}$$

where ϵ and μ are the electric permittivity and magnetic permeability, respectively. ρ and ρ^* are conductivity and magnetic conductivity, repectively. Assuming that there are no electric and magnetic currents in the free space, the system of equations can be written in the following form:

$$\frac{\partial \mathbf{U}}{\partial t} + \mathbf{A}\frac{\partial \mathbf{U}}{\partial x} + \mathbf{B}\frac{\partial \mathbf{U}}{\partial y} + \mathbf{C}\frac{\partial \mathbf{U}}{\partial z} = 0. \tag{9}$$

The one-dimensional, characteristic-based formulation is easily constructed from the eigenvalue and eigenvector analysis. The eigenvalues of the coefficient matrices $\mathbf{A}, \mathbf{B}$ and $\mathbf{C}$ are identical, but they contain multiplicities.

$$\mathrm{Diag}(\lambda) = \left\{ \frac{1}{\sqrt{\mu\epsilon}}, \frac{1}{\sqrt{\mu\epsilon}}, -\frac{1}{\sqrt{\mu\epsilon}}, -\frac{1}{\sqrt{\mu\epsilon}}, 0, 0 \right\}. \tag{10}$$

Then, the diagonization process is done to construct a non-singular similarity matrix and its left-hand inverse from the eigenvectors in each spatial dimension as followings:

$$D_x = S_x^{-1} A S_x \tag{11}$$
$$D_y = S_y^{-1} B S_y \tag{12}$$
$$D_z = S_z^{-1} C S_z, \tag{13}$$

where S is a non-singular similarity matrix constructed by the eigenvectors as the column vector and S^{-1} is its left-hand inverse. Similarity matrices associated with each of the coefficient matrices A, B and C are given by

$$S_x = \begin{bmatrix} 0 & 0 & 0 & 0 & 0 & 1 \\ \sqrt{\frac{\mu}{\epsilon}} & 0 & -\sqrt{\frac{\mu}{\epsilon}} & 0 & 0 & 0 \\ 0 & -\sqrt{\frac{\mu}{\epsilon}} & 0 & \sqrt{\frac{\mu}{\epsilon}} & 0 & 0 \\ 0 & 0 & 0 & 0 & 1 & 0 \\ 0 & 1 & 0 & 1 & 0 & 0 \\ 1 & 0 & 1 & 0 & 0 & 0 \end{bmatrix}, \tag{14}$$

$$S_y = \begin{bmatrix} -\sqrt{\frac{\mu}{\epsilon}} & 0 & \sqrt{\frac{\mu}{\epsilon}} & 0 & 0 & 0 \\ 0 & 0 & 0 & 0 & 1 & 0 \\ 0 & \sqrt{\frac{\mu}{\epsilon}} & 0 & -\sqrt{\frac{\mu}{\epsilon}} & 0 & 0 \\ 0 & 1 & 0 & 1 & 0 & 0 \\ 0 & 0 & 0 & 0 & 0 & 1 \\ 1 & 0 & 1 & 0 & 0 & 0 \end{bmatrix}, \tag{15}$$

$$S_z = \begin{bmatrix} \sqrt{\frac{\mu}{\epsilon}} & 0 & -\sqrt{\frac{\mu}{\epsilon}} & 0 & 0 & 0 \\ 0 & -\sqrt{\frac{\mu}{\epsilon}} & 0 & \sqrt{\frac{\mu}{\epsilon}} & 0 & 0 \\ 0 & 0 & 0 & 0 & 1 & 0 \\ 0 & 1 & 0 & 1 & 0 & 0 \\ 1 & 0 & 1 & 0 & 0 & 0 \\ 0 & 0 & 0 & 0 & 0 & 1 \end{bmatrix}, \tag{16}$$

where the ratio $\sqrt{\mu/\epsilon}$ is referred to the intrinsic impedance of the medium.

In the case that the permittivity and permeability are constant values, the left-hand inverse of the similarity matrix S^{-1} can be brought into the differentiation with respect to both time and space. The resulting equations are completely uncoupled from each other. These scalar equations describe the invariant characteristic variables along trajectories with slopes defined by their eigenvalues. Since, every equation is completely uncoupled each other, the system of equations can be solved individually in one-dimensional method. In this process, the CIP method is utilized to solve the system of equations. The characteristic variables

are advected forward or backward depending on the associated sign of its eigenvalue. All one-dimensional characteristic variables in each coordinate can be given as

$$W_x = S_x^{-1} U$$

$$S_x = \begin{bmatrix} 0 & \sqrt{\frac{\epsilon}{2\mu}} & 0 & 0 & 0 & \frac{1}{2} \\ 0 & 0 & -\sqrt{\frac{\epsilon}{2\mu}} & 0 & \frac{1}{2} & 0 \\ 0 & -\sqrt{\frac{\epsilon}{2\mu}} & 0 & 0 & 0 & \frac{1}{2} \\ 0 & 0 & \sqrt{\frac{\epsilon}{2\mu}} & 0 & \frac{1}{2} & 0 \\ 0 & 0 & 0 & 1 & 0 & 0 \\ 1 & 0 & 0 & 0 & 0 & 0 \end{bmatrix} ,(17)$$

$$W_y = S_y^{-1} U$$

$$S_y = \begin{bmatrix} -\sqrt{\frac{\epsilon}{2\mu}} & 0 & 0 & 0 & 0 & \frac{1}{2} \\ 0 & 0 & \sqrt{\frac{\epsilon}{2\mu}} & \frac{1}{2} & 0 & 0 \\ \sqrt{\frac{\epsilon}{2\mu}} & 0 & 0 & 0 & 0 & \frac{1}{2} \\ 0 & 0 & -\sqrt{\frac{\epsilon}{2\mu}} & \frac{1}{2} & 0 & 0 \\ 0 & 1 & 0 & 0 & 0 & 0 \\ 0 & 0 & 0 & 0 & 1 & 0 \end{bmatrix} ,(18)$$

$$W_z = S_z^{-1} U$$

$$S_z = \begin{bmatrix} \sqrt{\frac{\epsilon}{2\mu}} & 0 & 0 & 0 & \frac{1}{2} & 0 \\ 0 & -\sqrt{\frac{\epsilon}{2\mu}} & 0 & \frac{1}{2} & 0 & 0 \\ -\sqrt{\frac{\epsilon}{2\mu}} & 0 & 0 & 0 & \frac{1}{2} & 0 \\ 0 & \sqrt{\frac{\epsilon}{2\mu}} & 0 & \frac{1}{2} & 0 & 0 \\ 0 & 0 & 1 & 0 & 0 & 0 \\ 0 & 0 & 0 & 0 & 0 & 1 \end{bmatrix} .(19)$$

Therefore, in each coordinate direction, the time-dependent, three-dimensional Maxwell equations are uncoupled into six independent scalar equations according to their associated eigenvalues. For $n = 1, 2, \ldots, 6$,

$$L_x : \frac{\partial W_{x,n}}{\partial t} + \lambda_n \frac{\partial W_{x,n}}{\partial x} = 0, \qquad (20)$$

$$L_y : \frac{\partial W_{y,n}}{\partial t} + \lambda_n \frac{\partial W_{y,n}}{\partial y} = 0, \qquad (21)$$

$$L_z : \frac{\partial W_{z,n}}{\partial t} + \lambda_n \frac{\partial W_{z,n}}{\partial z} = 0. \qquad (22)$$

These equations are called the scalar Riemann equations, which can be solved individually by the CIP scheme described at the appendix of this paper.

Because the one-dimensional characteristics W_x, W_y, and W_z are distinct in different coordinates, a dependent variable transformation was performed during the computation to convert the characteristics from one
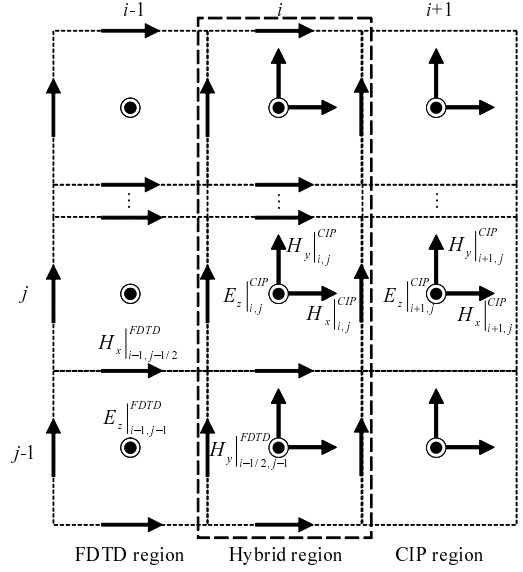
Figure 1: The arrangement of electric and magnetic field components around the boundary between FDTD and CIP regions

temporal-spatial plane to the other as following:

$$W_x = S_x^{-1} S_y W_y = S_x^{-1} S_z W_z, \qquad (23)$$

$$W_y = S_y^{-1} S_x W_x = S_y^{-1} S_z W_z, \qquad (24)$$

$$W_z = S_z^{-1} S_x W_x = S_z^{-1} S_y W_y. \qquad (25)$$

The three-dimensional system is solved by the fractional-step or time splitting scheme and the cyclic solving sequence of computation is given in the simple form as,

$$W^{n+1} = L_z L_y L_x W^n. \qquad (26)$$

3 Boundary Condition between CIP and FDTD region

In the present analysis, the FDTD method is used to implement current sources of antennas and the CIP method is applied for most of the analysis region which do not include the antenna. The FDTD method uses the leapfrog arrangement of electric and magnetic fields in the calculation but the field components in the CIP region are all at the same position in the cells, so that a new boundary condition between both regions is required to satisfy the continuity of the fields. The averaging method is utilized for the boundary condition in this paper. The arrangement of electric and magnetic fields around the proposed boundary condition is shown in Fig. 1. The field transition between both FDTD and CIP methods is occured at the position $i\Delta x$. First, the electric field components E_z of FDTD and CIP methods exist in the center of cells at the same position, so that the substutition can be done directly.

In order to obtain the magnetic field values $H_x|^{CIP}$ and $H_y|^{CIP}$ at the position $(i\Delta x, j\Delta y)$ in the hybrid region, the average value of the magnetic field components $H_x|^{CIP}$ and $H_y|^{CIP}$ are computed as followings:

$$E_z^n|_{i,j}^{CIP} = E_z^n|_{i,j}^{FDTD}, \tag{27}$$

$$H_x^n|_{i,j}^{CIP} = \frac{1}{2}\left(H_x^n|_{i,j-1/2}^{FDTD} + H_x^n|_{i,j+1/2}^{FDTD}\right), \tag{28}$$

$$H_y^n|_{i,j}^{CIP} = \frac{1}{2}\left(H_y^n|_{i-1/2,j}^{FDTD} + H_y^n|_{i-1/2,j}^{FDTD}\right), \tag{29}$$

where the averaging method is also applied for the magnetic field components $H^{n-1/2}$ and $H^{n+1/2}$ because these components in the FDTD region do not exist in the temporal step n. After all of electric and magnetic field components are retrived from the FDTD region, the CIP method is used to calculate the fields in the CIP region. It is neccessary to note that the hybrid region was not included in the field calculation in this process, but its field values was applied for the computation of all field components at the position $((i+1)\Delta x, j\Delta y)$ in the CIP region. Then, the electric field component $E_z|_{i+1,j}^{CIP}$ is utilized to calculate the magnetic field $H_y|_{i+1/2,j}^{FDTD}$ by the ordinary Yee's algorithm as the following update equation:

$$H_y^{n+1/2}\Big|_{i+1/2,j}^{FDTD} = H_y^{n-1/2}\Big|_{i+1/2,j}^{FDTD} \\ + \frac{\Delta t}{\mu\Delta x}\left(E_z^n|_{i+1,j}^{CIP} - E_z^n|_{i,j}^{FDTD}\right). \tag{30}$$

The electric and magnetic field components in the both analysis regions are all computed at this process. It is important to save the magnetic field values of the last computation because the temporal averaging must be done before the CIP calculation starts in the next step. Finally, the cyclic computation are done until the required time step N was reached.

Numerical simulations of the present CIP-FDTD method are performed in a truncated computational domain defined by a two-dimensional plane. The size of the plane is 800×400 cells. A half of the analysis space is the FDTD region, and the other is the CIP region. The cell size Δx and Δy are 6 millimeters in both regions. The FDTD and CIP regions are seperated each other by the proposed boundary at the center as illustrated in Fig. 2. Two points s_1, s_2 are defined to observe the waveform at the location $x = 390\Delta x$, and $410\Delta x$. The reflection and transmission coefficient were calculated to validate our proposed method. To determine the quantity of electric fields which are reflected from the boundary, an incident gaussian plane wave was induced at $x = 350\Delta x$ in the FDTD region. The first-order Mur's absorbing boundary condition was utilized to terminate the trancated space at the left and right boundary illustrated in the Fig 2. For the top and bottom boundary, the one-dimensional

$$E_z^{inc}(x) = \exp\left(-\frac{1}{\rho^2}(x-1.95)^2\right), \quad \rho = 0.036[m]$$
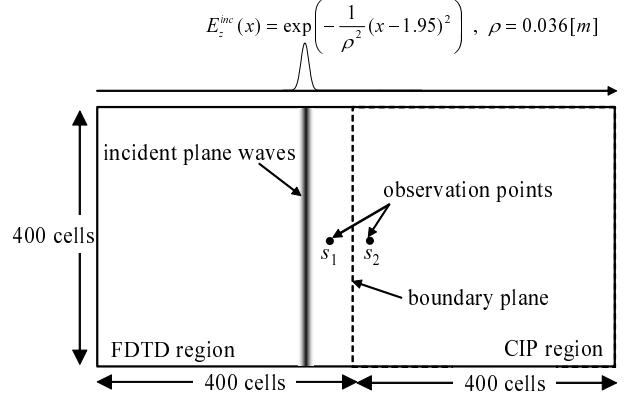
Figure 2: Analysis model for the calculation of reflection from the boundary

FDTD calculation of the same model was performed to create a perfect continuous plane-wave condition. The following equations were applied to calculate the field quantity reflected from the boundary and the quantity propagated from the FDTD region into the CIP region through the boundary.

$$R = 20\log_{10}\left|\frac{\mathcal{F}\left(E_z^{FDTD} - E_z^{CIP}\right)}{\mathcal{F}(E_z^{inc})}\right|, \tag{31}$$

$$T = 1 - R = 20\log_{10}\left|\frac{\mathcal{F}(E_z^{CIP})}{\mathcal{F}(E_z^{inc})}\right|, \tag{32}$$

where $\mathcal{F}(x)$ implies the Fourier transformation of variable x. E_z^{FDTD} and E_z^{CIP} were obtained by the observation at the points s_1 and s_2 respectively. Note that both of the reflection and transmission coefficients were normalized by the incident field.

The numerical result of the refection and transmission coefficients is shown in Fig. 3. The result shows that the reflection coefficient increases as the frequency increases over broad ranges. The result shows that the electromagnetic waves can propagate from the FDTD region across the proposed boundary with the reflection coefficient smaller than -30dB below 10GHz in the case the cell size Δx is equal to 0.001[m]. The result also shows that the reflection coefficient increases as the cell size increases by about the same ratio.

4   Numerical dispersion error

To investigate the numerical dispersion errors of each computation method, the incident field was applied in the center of analysis space. The size of the analysis space is 400×400 cells with the same cell sizes $\Delta x = \Delta y = 6[mm]$ as that described in the previous section. There is no need to trancate the analysis space with any boundary condition because every calculation was stopped before the field waves reaches the boundary. The discrete Fourier transform was performed at every point of calculation for the frequency

4
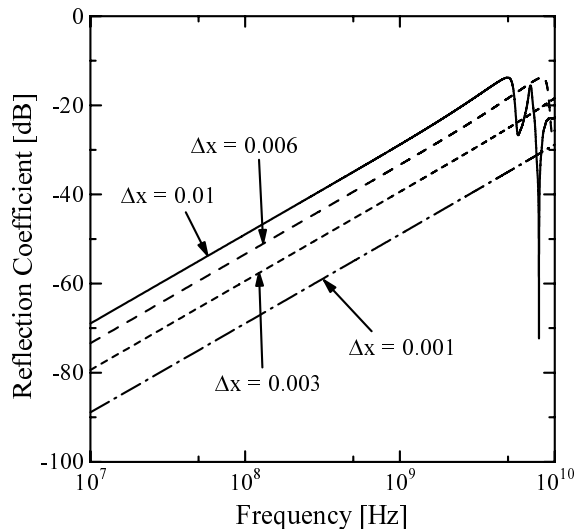
Figure 3: Reflection coefficients of the CIP/FDTD boundary

Figure 4: Numerical phase velocity versus propagation angle at $\lambda = 10\Delta x$

from 0.5GHz to 10GHz with 0.5GHz interval. The results of the numerical error are shown in the Fig. 4 and Fig. 5.

The results show the numerical phase velocity with different propagation angles at $0°$, $30°$ and $45°$ direction in a two-dimensional analysis space. From the results, the error accumulation of the FDTD and CIP method have an inverse characteristic: the worse-case velocity error is occured at $45°$ direction in the FDTD method, but the error accumulation is smallest in the $0°$ direction as illustrated in the figures. The results in the cases of $\Delta = \lambda_0/20$, $\lambda_0/10$ and $\lambda_0/5$ are summarized in the Table 1. The worst-case velocity error of the FDTD method for $\Delta = \lambda_0/5$ grid solution is -8.3%, but the error declines to only -0.62% for $\Delta = \lambda_0/20$ at the $45°$ direction of propagation. That means that for the former case, a sinusoidal numerical wave traveling over a $10\lambda_0$ distance would develop a lagging phase error of about $149.45°$. These accumulative errors may be troublesome for the analysis of scattering structures involving phase cancellation such as the propagation characteristic analysis of MIMO (multiple-input multiple output) system. On the other hand, the CIP method has a superior characteristic of dispersion error. The lagging phase for $10\lambda_0$ distance of propagation is only $66.9°$ in the worst case which is about 44.7 percents smaller than that of the FDTD method.

As a result, the CIP-FDTD method has the similar characteristic of the numerical dispersion to the CIP method in a wide range of analysis frequency. The numerical phase velocity versus propagation angle in the cases $\lambda = 10\Delta x$ and $\lambda = 5\Delta x$ are shown in Fig. 4 and Fig. 5, respectively. In the case $\lambda = 10\Delta x$, the worst case in the FDTD scheme is occured at $\theta = 0°$, which is about 1% delaying from the normal light

Table 1: The comparison of numerical phase errors between each method

		phase errors per wavelength[deg.]		
		FDTD	CIP	CIP-FDTD
$\lambda = 25\Delta x$	0°	0.88	0.38	0.36
	30°	0.53	0.62	0.56
	45°	0.40	0.69	0.62
$\lambda = 10\Delta x$	0°	3.44	0.27	0.29
	30°	1.12	1.54	1.51
	45°	0.32	1.94	1.90
$\lambda = 5\Delta x$	0°	14.94	0.52	0.59
	30°	4.62	5.36	5.12
	45°	0.48	6.76	6.69

velocity in the vacuum. However, the worst case of CIP and CIP-FDTD scheme is occured at $\theta = 45^o$, with the phase velocity error about 0.5% which is a half smaller than FDTD result. Hereby, it was proved that the CIP-FDTD has a superior propagation characteristic than that of FDTD scheme.

5 Concluding remarks

In this paper, the hybrid CIP-FDTD method was developed as a new technique combining the CIP method and the FDTD method to solve a problem of the large- or long-distance propagation with an antenna included in the analysis space. The design of the boundary conditions between the FDTD method and the CIP method was implemented to maintain the continuity of the fields by utilizing the averaging value of magnetic
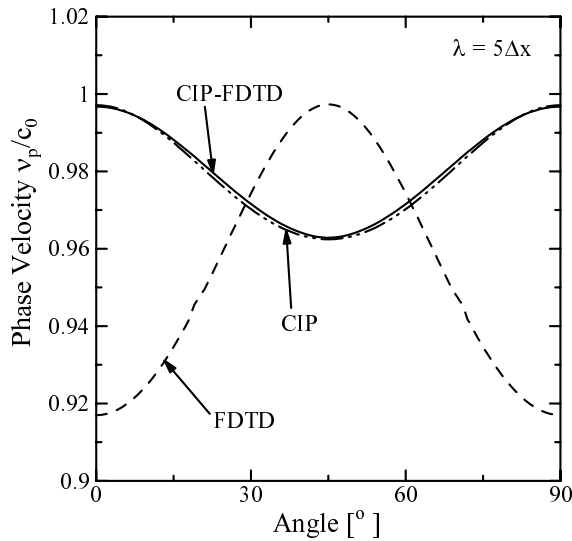
Figure 5: Numerical phase velocity versus propagation angle at $\lambda = 5\Delta x$

fields. The reflection coefficient of the electric fields is consequently about -20dB or less below 4GHz in the case that an incident field is applied in the FDTD region. The boundary condition is validated and able to be realized to 4GHz. Furthermore, the numerical dispersion of the CIP-FDTD method was investigated. The results verify that the CIP-FDTD method has the similar characteristic to that of the CIP method. This method can be extended to the three-dimensional hybrid case that would be further researched in the future.

References

[1] K.S.Yee, "Numerical Solution of Initial Boundary Value Problems Involving Maxwell ' s Equations in Isotropic Media," IEEE Trans. Antennas Propagat., vol.14, no.4, pp.302-307, 1996

[2] J. Jin, "The Finite Element Method in Electromagnetics" IEEE Press, 1996

[3] Roger F.Harrington, "Field computation by moment methods" IEEE Press, 1993

[4] A. Taflove, "Computational Electrodynamics, The Finite-Difference Time-Domain Method" Artech House Publisher, 1995

[5] M.F.Fadi and M.Piket-May, "A Modified FDTD(2,4) scheme for modeling electrically large structures with high-phase accuracy," IEEE Trans. Antennas Propagat., vol.45, no.2, pp.254-264, 1997

[6] K.Lan, Y.Liu, and W.Lin, "A Higher Order (2,4) Scheme for Reducing Dispersion in FDTD Algorithm," IEEE Trans. Electromagn. Compat., vol.41, no.2, pp.160-165, may 1999

[7] C.W.Manry Jr, S.L.Broschat, and J.B.Schneider, "Higher-Order FDTD Methods for Large Problems," J.Appl. Comput. Electromag. Soc., vol.10, no.2, pp.17-29, 1995

[8] Y.Ogata, T.Yabe, K.Odagaki, "An Accurate Numerical Scheme for Maxwell Equation with CIP-Method of Characteristics," Commun. Comput. Phys., vol.1, no.2, pp.311-335, april 2006

[9] T.Nakamura, R.Tanaka, T.Yabe, K.Takizawa, "Exactly Conservative Semi-Lagrangian Scheme for Multi-dimensional Hyperbolic Equations with Directional Splitting Technique," J. Comput. Phys., vol.174, pp.171-207, 2001

[10] F.Xiao, T.Yabe, "Completely Conservative and Oscillationless Semi-Lagrangian Schemes for Advection Transportation," J. Comput. Phys., vol.170, pp.498-522, 2001

[11] T.Utsumi, T.Kunugi, T.Aoki, T.Yabe, "Stability and accuracy of the Cubic Interpolated Propagation scheme," Comput. Phys. Commun., vol.101, pp.9-20, 1997

[12] T.Yabe, K.Takizawa, M.Chino, M.Imai, and C.C.Chu, "Challenge of CIP as a universal solver for solid liquid and gas," Int. J. Numer. Methods Fluids, vol.47, pp.655-676, 2005

[13] S.Watanabe, O.Hashimoto, "An Examination about Method for Analyzing Electromagnetic Field Using CIP Method," IEICE Tech. Report, EMCJ2005-37, pp.91-95, June 2005

[14] Y.Yoshida, K.Okubo, N.Takeuchi, "The Type-C CIP Electromagnetic Field Analysis," IEICE Tech. Report, AP2006-70, pp.7-12, September 2006

[15] K.Okubo, N.Takeuchi, "Numerical Analysis of Electromagnetic Field Generated by Line Current Using the CIP Method," IEICE Tech. Report, AP2004-336, pp.197-202, March 2005

[16] K.Okubo, N.Takeuchi, "A Consideration on Application of Time Domain Numerical Analysis Using CIP Method to Electromagnetic Fields," IEICE Tech. Report, AP2005-84, pp.7-12, October 2005

[17] J.S.Shang, "A Fractional-Step Method for Solving 3D, Time-Domain Maxwell Equations," J. Comp. Phys., vol.118, pp.109-119, 1995